International Journal of Automotive Technology, Vol. 16, No. 4, pp. 593–601 (2015)
DOI 10.1007/s12239–015–0060–z

pISSN 1229–9138/ eISSN 1976–3832

ATTITUDE MOTION CONTROL OF THE ACTIVE SUSPENSION SYSTEM WITH TRACKING CONTROLLER

I. YOUN[1)*], L. WU[1)], E. YOUN[1)] and M. TOMIZUKA[2)]

[1)]Department of Mechanical Engineering, ReCAPT, Gyeongsang National University, Gyeongnam 660-701, Korea
[2)]Department of Mechanical Engineering, University of California, Berkeley, CA 94720, USA

(Received 12 May 2014; Revised 28 November 2014; Accepted 3 January 2015)

ABSTRACT–This research focuses on the attitude motion controller to improve the ride-comfort and handling capability of a vehicle simultaneously. The attitude tracking controller is designed to let the actual motion of the car body follow the ideally guided value, which is developed conceptually to eliminate lateral and longitudinal forces acting on passengers. The tracking control forces are computed based on the three predicted data proposed for the future ideal roll and pitch motions. In conventional ways, the car body leans outside around sharp turns because of the centrifugal force and it dives forward when braking and leans back when accelerating. However, the attitude tracking controller makes the car body skew inside at cornering, squat at braking, and dive at accelerating. Simulations are performed based on a four degree-of-freedom half car model and then the results show the great potential of the proposed approach.

KEY WORDS : Attitude motion, Tracking control, Ride-comfort, Handing capability

1. INTRODUCTION

Ride-comfort and handling capability have been considered as conflicting goals in designing controllers for active and semi-active suspension systems as long as dynamic performance of a car reacting against road disturbance is concerned (Youn and Hac, 2006; Cho *et al*., 2005; Malekshahi and Mirzaei, 2012). The conventional concepts on ride-comfort and handling capability said that up and down vibration of vehicle body caused by road elevation worsens ride-comfort and handling capability is related to ground grasping force of tire (Youn, 1992). When the vehicle is accelerating, braking, cornering, or traveling on tilted roads, longitudinal forces acting on passengers during the braking and accelerating activities and lateral forces at the corners deteriorate both ride-comfort and handling capability simultaneously. The two design goals can be improved together in case of controlling attitude motion of a vehicle. If the attitude motion controller reduces the unpleasant accelerations that occur when accelerating, decelerating, or turning at sharp corners, it may also make handling capability much better because of the balanced weight distribution achieved by the proper combination of lateral and longitudinal forces and mass shift. Reducing roll motion of car body is widely studied by using anti-roll bar, as (Gaspar *et al*., 2005). However, leaning car body in the opposite direction of a passive vehicle at cornering, braking and accelerating is a more effective method for improving ride-comfort and handling capability. 'Active tilting technology' was well established in modern high speed railway vehicles with active tilt systems (Goodall, 1999). For road vehicles, enhancement of ride-comfort and handling capability by tilting the vehicle inward in cornering was carried out and the tilting angle is determined by the roll moment of passive vehicle. In this way, accelerations on passengers can be reduced about 30% (Wang and Shen, 2008). Whereas, the experimental results showed that the minimum acceleration at which a passenger feels discomfort is 0.25 g (Wu *et al*., 2009). Usually, passengers feel no worries as long as the longitudinal acceleration is less than 0.1 g (Shen *et al*., 2000). Obviously ride-comfort should be improved more by tilting car body to the proposed desired roll and pitch angles which are obtained by the given method in this work to balance out the longitudinal and lateral forces. In the previous research, the optimal controller using integral action for the suspension deflection considerably reduced the roll and the pitch motions at sharp corners and braking manoeuvres (Youn *et al*., 2006). Unlike the prior research work regarding the attitude control, which utilized the feedback control only to keep zero pitch and roll angle of the car body as much as possible, the proposed attitude controller uses the feedback and feed-forward controller to follow the ideal pitch and roll angles of car body. In other words, the tracking controller, which is designed to minimize the variance of difference between actual and desired outputs, helps the

**Corresponding author.* e-mail: iyoun@gnu.ac.kr

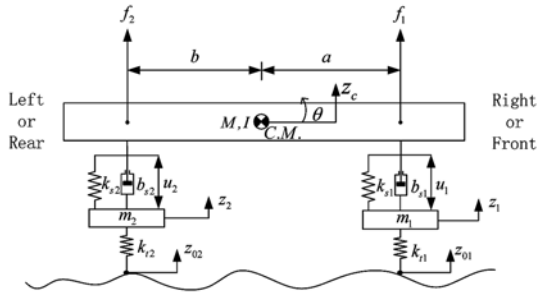

Figure 1. Simple mathematical dynamic model of a longitudinal or lateral half car.

vehicle's body to lean in the opposite direction of the rollover at cornering. The controller also keeps the car in squatting position when decelerating and in diving position when accelerating. In that way, the proposed algorithms can improve simultaneously both ride-comfort and handling capability which are generally known as conflicting design goals. The attitude controller that consists of feedback and feed-forward parts achieves the calculated ideal posture of the vehicle while running under various situations.

2. PROBLEM FORMULATION

A simple four degree of freedom mathematical model based on a half car shown in Figure 1 is used in this attitude motion control study. The dynamic equations of motion are given for a lateral half car model as

$$M\ddot{z}_c = f_r + f_1 + f_l + f_2 \tag{1}$$

$$I\ddot{\theta} = (f_r + f_1)a - (f_l + f_2)b \tag{2}$$

$$m_1\ddot{z}_1 = -k_{t1}(z_1 - z_{01}) - f_r \tag{3}$$

$$m_2\ddot{z}_2 = -k_{t2}(z_2 - z_{02}) - f_l \tag{4}$$

Where,

$$f_r = k_{s1}(z_1 - z_c - a\theta) + b_{s1}(\dot{z}_1 - \dot{z}_c - a\dot{\theta}) + u_1 \tag{5a}$$

$$f_l = k_{s2}(z_2 - z_c + b\theta) + b_{s2}(\dot{z}_2 - \dot{z}_c + b\dot{\theta}) + u_2 \tag{5b}$$

In above equations M and I are the sprung mass and its moment of inertia, respectively, m_1 and m_2 are the right and left unsprung masses, and u_1 and u_2 are the control forces. The parameters, k_{s1}, k_{s2} and b_{s1}, b_{s2} denote the stiffness and damping coefficients of passive suspension elements for right and left assembles. Similarly, k_{t1} and k_{t2} denote the right and left tire stiffness. The given model can be considered as a longitudinal half car when simulating braking and accelerating motions and a lateral one when examining the cornering motion of a car.

The desired posture of a car leans in the opposite

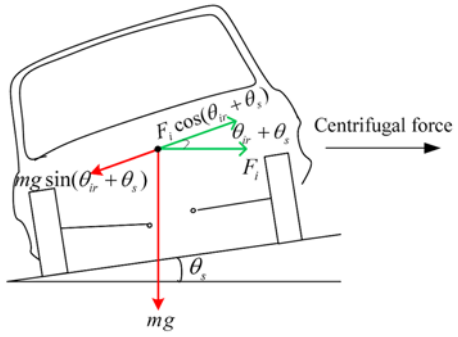

Figure 2. Ideal attitude motion of a vehicle turning and braking on a banked circular road.

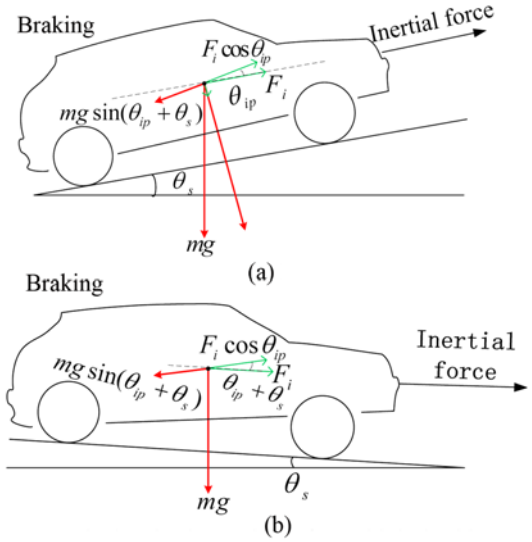

Figure 3. Ideal attitude motion of a vehicle braking on (a) an uphill road and (b) a downhill road.

direction of the rollover at cornering on banked roads. Figure 2 shows that the ideal roll angle of a car body relative to banked road angle can be determined by equation (6). Figure 3 shows that the ideal pitch angles relative to slope during the brake or the acceleration on ramp road are decided by equations, (7a) and (7b), and the desired pitch angle increase in opposite to leaning or diving direction of a car occurred at accelerating or braking. When the car has zero acceleration, the ideal pitch posture of the car body on uphill will be parallel to the road slope and on downhill will be parallel to the horizontal plane according to equations (7a) and (7b), respectively.

For desired roll angle:

$$\begin{aligned} & mg\sin(\theta_{ir} + \theta_s) = ma_{ac}\cos(\theta_{ir} + \theta_s) \\ & \Rightarrow \frac{a_{ac}}{g} = \tan(\theta_{ir} + \theta_s) = \frac{\tan\theta_{ir} + \tan\theta_s}{1 - \tan\theta_s \tan\theta_{ir}} \\ & \theta_{ir} = arctan\left(\frac{a_{ac} - g\tan\theta_s}{a_{ac}\tan\theta_s + g}\right) \end{aligned} \tag{6}$$

For desired pitch angle:

$$\begin{aligned}&\text{If } \theta_s \geq 0 \text{ ,}\\ &mg \sin \theta_{ip} \cos\theta_s = F_i \cos \theta_{ip}\\ &\Rightarrow \frac{a_{ac}}{g} = \frac{\sin\theta_{ip}\cos\theta_s}{\cos\theta_{ip}} = \tan\theta_{ip}\cos\theta_s\\ &\theta_{ip} = \arctan\left(\frac{a_{ac}}{g\cos\theta_s}\right), \text{ where } F_i = ma_{ac}\end{aligned} \tag{7a}$$

$$\begin{aligned}&\text{If } \theta_s < 0 \text{ ,}\\ &mg \sin(\theta_{ip}+\theta_s) = F_i \cos \theta_{ip}\\ &\Rightarrow \frac{a_{ac}}{g} = \frac{\sin(\theta_{ip}+\theta_s)}{\cos\theta_{ip}} = \tan\theta_{ip}\cos\theta_s + \sin\theta_s\\ &\theta_{ip} = \arctan\left(\frac{a_{ac}}{g\cos\theta_s}\right) - \theta_s, \text{ where } F_i = ma_{ac}\end{aligned} \tag{7b}$$

α_{ac} in equation (6) is the centrifugal acceleration at cornering and α_{ac} in equations (7a) and (7b) is the inertia acceleration at braking or accelerating, g is gravitational acceleration, m is the mass of a car body, a driver, or a passenger, and θ_s is the gradient of road surface. F_i is the inertia force and the opposite direction to acceleration of the car. θ_{ir} and θ_{ip} represent the ideal roll and pitch angles of the car body, respectively. Conceptually, those ideal angles are derived to eliminate the lateral and longitudinal forces acting on passengers by using the way in which the gravitational force acting on the passengers counterbalances the lateral and longitudinal forces in terms of passengers except normal forces. During the attitude motion, the hypothetical body forces acting on the suspension mounting points of the both sides have the same magnitude and are in opposite direction to each other. Considering the conditions that the car is running on a banked road in the circular path and a ramp road, the magnitudes of the hypothetical body forces in roll and pitch motions are shown by equations (8) and (9), respectively.

$$|f_{r1,2}| = \left| m\left(\frac{v^2}{r}cos\,\theta_s - g\ sin\,\theta_s\right)\cdot\frac{h}{a+b}\right| \tag{8}$$

$$|f_{p1,2}| = \left| (F_i - mg\sin\theta_s)\cdot\frac{h}{a+b}\right| \tag{9}$$

In equations (8) and (9), v is the car speed, r is the radius of road curvature, and h is the distance from the mass center of car body to road surface. a and b are the distances from the mass center to the two mounting points, respectively.

3. CONTROL STRATEGY

In order to design the controller, the system dynamic states have to be selected by the control designer after considering the possible sensors applicable to the system, the variables to control, the easiest way to formulate, and so on. In this work, the state vector and the disturbance input vector, which contains road disturbance and body forces applying to mounting points, are defined in equation (10) and (11), respectively. The desired state vector, $\mathbf{x_d}$, which contains the ideal pitch or roll angle, is represented in equation (12).

$$\mathbf{x} = [z_c, \dot{z}_c, \theta, \dot{\theta}, z_1 - z_{01}, \dot{z}_1, z_2 - z_{02}, \dot{z}_2, z_1, z_2]^T \tag{10}$$

$$\mathbf{w} = [\dot{z}_{01}, \dot{z}_{02}, f_1, f_2]^T \tag{11}$$

$$\mathbf{x_d} = [0, 0, \theta_d, 0, 0, 0, 0, 0, 0, 0]^T \tag{12}$$

The dynamic equations of motion can be expressed by the continuous time state space vector equation with the inputs, such as control forces, road disturbance velocities, and body forces with **A**, **B** and **D** given by Appendix.

$$\dot{\mathbf{x}} = \mathbf{Ax} + \mathbf{Bu} + \mathbf{Dw} \tag{13}$$

The active tracking optimal controller minimizes the performance index (14) that compromises the heave and roll (or pitch) accelerations representing ride-comfort, suspension rattle space, the difference between desired and actual angles of the car body, road holding forces, and control forces.

$$\begin{aligned}J = \lim_{T\to\infty}\frac{1}{2T}\int_0^T [&\rho_1\dot{x}_2^2 + \rho_2\dot{x}_4^2 + \rho_3(x_1 + ax_3 - x_9)^2\\ &+ \rho_3(x_1 - bx_3 - x_{10})^2 + \rho_4(x_{d_3} - x_3)^2\\ &+ \rho_3 x_5^2 + \rho_5 x_7^2 + \rho_6 u_1^2 + \rho_6 u_2^2\ ]dt\end{aligned} \tag{14}$$

Using equations (1) ~ (4), the definitions of the state vector (10), the disturbance vector (11), and the desired state vector (12), the performance index (14) can be expressed in forms of the matrices and the vectors which represent the errors between the desired states and the system states, disturbance inputs, and control forces.

$$\begin{aligned}J(\mathbf{x},\mathbf{u},\mathbf{w}) = \lim_{T\to\infty}\frac{1}{2T}\int_0^T [&(\mathbf{x_d}-\mathbf{x})^T\boldsymbol{Q}(\mathbf{x_d}-\mathbf{x})\\ &+ 2(\mathbf{x_d}-\mathbf{x})^T\mathbf{N_1}\mathbf{u} + 2(\mathbf{x_d}-\mathbf{x})\mathbf{N_2}\mathbf{w} + \mathbf{u}^T\mathbf{R}\mathbf{u}\\ &+ 2\mathbf{w}^T\mathbf{M_1}\mathbf{u} + \mathbf{M_2}\mathbf{w}]dt\end{aligned} \tag{15}$$

With $\mathbf{Q}$, $\mathbf{N_1}$, $\mathbf{N_2}$, $\mathbf{R}$, $\mathbf{M_1}$ and $\mathbf{M_2}$ specified by Appendix. Assume that $\mathbf{x_d}(\hat{o})$, $\tau \in [t, t+t_p]$, is known deterministically. If the pair ($\mathbf{A_n}$, $\mathbf{B}$) is stabilizable and ($\mathbf{A_n}$, $\mathbf{Q_n}^{1/2}$) is detectable, then the optimal tracking control law that minimizes $\boldsymbol{J}$ is derived by Appendix.

$$\mathbf{u} = -\mathbf{R}^{-1}[(\mathbf{B}^T\mathbf{P} - \mathbf{N_1}^T)\mathbf{x} + \mathbf{M_1}^T\mathbf{w} + \mathbf{N_1}^T\mathbf{x_d} + \mathbf{B}^T\mathbf{g_R}] \tag{16}$$

where $\mathbf{P}$ is a positive definite solution of the algebraic Riccati equation.

$$0 = \mathbf{A_n}^T\mathbf{P} + \mathbf{P}\mathbf{A_n} - \mathbf{P}\mathbf{B}\mathbf{R}^{-1}\mathbf{B}^T\mathbf{P} + \mathbf{Q_n} \tag{17}$$

And the vector $\mathbf{g_R}(t)$ satisfies

$$\begin{aligned}\mathbf{g_R}(t) = \int_0^{t_p} e^{-\mathbf{A_c}^T\tau}[&(\mathbf{P}\mathbf{D_n} - \mathbf{N_n})\mathbf{w}(\tau)\\ &-(\mathbf{Q_n} + \mathbf{P}\mathbf{B}\mathbf{R}^{-1}\mathbf{N_1}^T)\mathbf{x_d}(\tau)]d\tau\end{aligned} \tag{18}$$

where,

$$\mathbf{A_n}=\mathbf{A}+\mathbf{B}\mathbf{R}^{-1}\mathbf{N}_1^T,\ \mathbf{A_c}=\mathbf{A_n}-\mathbf{B}\mathbf{R}^{-1}\mathbf{B}^T\mathbf{P}$$
$$\mathbf{Q_n}=\mathbf{Q}-\mathbf{N}_1\mathbf{R}^{-1}\mathbf{N}_1^T,\ \mathbf{N_n}=\mathbf{N}_2-\mathbf{N}_1\mathbf{R}^{-1}\mathrm{M}_1^T \quad (19)$$
$$\mathbf{D_n}=\mathbf{D}-\mathbf{B}\mathbf{R}^{-1}\mathbf{M}_1^T$$

Where $\mathbf{A_c}$ is the closed loop system matrix that is asymptotically stable. The optimal tracking controller (16) is composed of a feedback part, $-\mathbf{R}^{-1}[(\mathbf{B}^T\mathbf{P}-\mathbf{N}_1^T)\mathbf{x}+\mathbf{M}_1^T\mathbf{w}+\mathbf{N}_1^T\mathbf{x_d}]$, which is the same as in the corresponding problem without the preview information of disturbances and the predicted data for desired states, and a feed-forward part, $-\mathbf{R}^{-1}\mathbf{B}^T\mathbf{g_R}$, which depends on the future ideal angles of the car body in addition to the future road disturbances and body forces which are not considered in this work.

The optimal steady state solution which is given above is limited in case of an optimal tracking control problem with a finite time range. That is the problem of minimizing

$$J(\mathbf{x},\mathbf{u},\mathbf{w})=E\ \{\frac{1}{2}(\mathbf{x}_{d_T}-\mathbf{x}_T)^T\mathbf{S}(\mathbf{x}_{d_T}-\mathbf{x}_T)$$
$$+\frac{1}{2}\int_0^T[(\mathbf{x_d}-\mathbf{x})^T\mathbf{Q}(\mathbf{x_d}-\mathbf{x})+2(\mathbf{x_d}-\mathbf{x})^T\mathbf{N}_1\mathbf{u} \quad (20)$$
$$+2(\mathbf{x_d}-\mathbf{x})^T\mathbf{N}_2\mathbf{w}+\mathbf{u}^T\mathbf{R}\mathbf{u}+2\mathbf{w}^T\mathbf{M}_1\mathbf{u}+\mathbf{w}^T\mathbf{M}_2\mathbf{w}]dt\}$$

Subject to dynamic constraint (13), $\mathbf{S}$ is a symmetric, non-negative definite matrix. In this case, the optimal tracking controller has the form given by equation (16) with time dependent matrix $\mathbf{P}(t)$ which is a solution of the Riccati equation

$$-\dot{\mathbf{P}}=\mathbf{A}_n^T\mathbf{P}+\mathbf{P}\mathbf{A}_n-\mathbf{P}\mathbf{B}\mathbf{R}^{-1}\mathbf{B}^T\mathbf{P}+\mathbf{Q_n} \quad (21)$$

And the vector satisfying

$$\dot{\mathbf{g}}_R=-\mathbf{A}_c^T\mathbf{g}_R-(\mathbf{P}\mathbf{D_n}-\mathbf{N_n})\mathbf{w}+(\mathbf{Q_n}+\mathbf{P}\mathbf{B}\mathbf{R}^{-1}\mathbf{N}_1^T)\mathbf{x_d} \quad (22)$$

where, $\mathbf{g}_R(T)=0$

Finally, substituting the optimal tracking control force (16) into the linear state space equation (13), the closed loop system equation can be written by

$$\dot{\mathbf{x}}=\mathbf{A_c}\mathbf{x}+\mathbf{D_n}\mathbf{w}-\mathbf{B}\mathbf{R}^{-1}\mathbf{N}_1^T\mathbf{x_d}-\mathbf{B}\mathbf{R}^{-1}\mathbf{B}^T\mathbf{g}_R \quad (23)$$

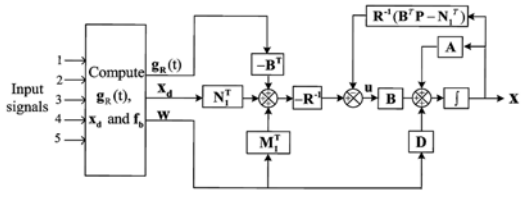

signal 1: Braking force, signal 2: accelerating force, signal 3: vehicle velocity, signal 4: radius of curvature, signal 5: road disturbance

Figure 4. Block diagram for the attitude motion control strategy with tracking controller.

The more detailed derivation for the optimal tracking controller design in continuous time is shown in Appendix.

Figure 4 shows the block diagram for the attitude motion control strategy in which the present desired roll and pitch angles are obtained by using the input signals and the future desired angles can be predicted by previously mentioned methods and finally $\mathbf{g}_R$ can be computed by the predicted data. In that way, the feed-forward part can be obtained. The control force consists of the feed-forward part and the feedback part as shown in Figure 4.

4. FREQUENCY CHARACTERISTICS

The frequency domain characteristics of the lateral or longitudinal half car model can be obtained by taking the Fourier transform of the closed loop equation (23).

$$\frac{X(j\omega)}{w(j\omega)}=(j\omega\ \mathbf{I}-\mathbf{A}_c)^{-1}\mathbf{D}_n\cdot[e^{-j\omega\tau_1}\ e^{-j\omega\tau_2}\ 0\quad 0]^{\mathrm{T}} \quad (24)$$

Through $|X(j\omega)/w(j\omega)|$, the amplitude ratio of the car body motions against the road input can be obtained without considering the body force and the desired angle. Therefore, f_1, f_2, and $\mathbf{x_d}$ are zeros and the preview information of the road input is not concerned in this work, either. Two types of road inputs are utilized to obtain frequency characteristics. The inputs to the two wheels are in phase for heaving input, as $e^{-j\omega\tau 1}=e^{-j\omega\tau 2}=1$, whereas the inputs applied to two wheels are opposite in phase for pitch or roll input, as $e^{-j\omega\tau 1}=1$, $e^{-j\omega\tau 2}=-1$. The frequency domain characteristics show how much the weighting factor for the desired motion of the car body in the performance index (14) deteriorates ride-comfort and road holding capability. By using the frequency domain characteristics, the proper weighting factors can be determined to obtain the optimal tracking controller.

5. SIMULATION RESULTS AND ANALYSIS

In this section, the cases of roll and pitch motions related to vehicle motional attitude are discussed based on lateral and longitudinal 4-DOF half car models. The vehicle parameters and the weighting factors that are used in the simulation are listed in Table 1 and Table 2.

After the weighting factors in the performance index, excluding ρ_4, were determined prioritizing the enhancement of the ride-comfort, ρ_4 was determined utilizing the frequency characteristics.

As shown in Figure 5, different values of ρ_4, which penalize the difference between the desired and the actual angles of the car body, have varying effects on the frequency characteristics. The value of 10^5 is selected as a proper value of ρ_4 because the value can get the great advantage of tracking ability in addition to better ride-comfort capability with some deterioration of suspension deflection as shown in Figure 5 (a). The value of ρ_4 does not influence the heave motion of the vehicle as shown in

Table 1. Parameter values of 4-DOF longitudinal and lateral half car models.

Symbols	Lateral half car model	Longitudinal half car model
M	500[kg]	500[kg]
I	200[kg.m^2]	1222[kg.m^2]
m_1,m_2	25[kg]	25[kg]
k_{s1},k_{s2}	18[kN/m]	18[kN/m]
k_{t1},k_{t2}	180[kN/m]	180[kN/m]
b_{s1},b_{s2}	1[kN s/m]	1[kN s/m]
a	0.74[m]	1.25[m]
b	0.74[m]	1.51[m]
h	0.7[m]	0.7[m]

Table 2. Weighting factor.

Weighting factor	Targets	Value
ρ_1	Heaving acceleration	1
ρ_2	Roll/pitch angular acceleration	1
ρ_3	Suspension deflection	10^3
ρ_4	Error between desired and actual roll/pitch angle	10^5
ρ_5	Tire deflection	10^4
ρ_6	Control force	10^{-6}

Figure 5 (b).

This research introduces three different methods to obtain the predicted data of the desired values, $\theta_d(t+t_p)$, $t_p \in [0, 0.3]$. Briefly speaking the basic concepts, if the future ideal roll and pitch angles are known completely, the most ideal control force can be computed for the proposed tracking controller. Therefore, the known future data are used first. However, it is not realistic. Two other practical ways to predict the future ideal roll and pitch angles are also proposed in this paper:

Method 1) $\theta_d(t+t_p)$ is the known predicted data, which is assumed to be already known.

Method 2) $\theta_d(t+t_p)$ is the gradient predicted data, which is estimated by using the gradient at present time with an angle limit of 45° as the following:

$$\theta_d(t+t_p) = \dot{\theta}_d(t) \cdot t_p + \theta_d(t)$$
$$if\ \theta_d(t+t_p) < -45^\circ,$$
$$\theta_d(t+t_p) = -45^\circ$$
$$if\ \theta_d(t+t_p) > 45^\circ,$$
$$\theta_d(t+t_p) = 45^\circ$$

Method 3) $\theta_d(t+t_p)$ is the constant predicted data, which is considered to be the same as the desired value at present

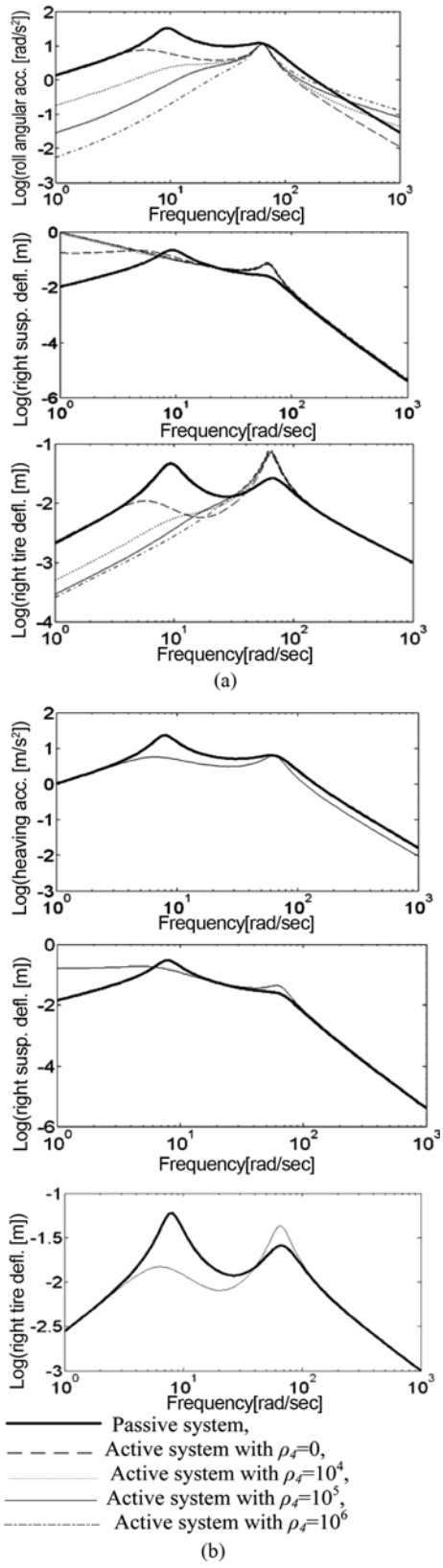

Figure 5. Frequency characteristics of a lateral half car model obtained by (a) roll road input and (b) heave road input.

time as the following:

$$\theta_d(t + t_p) = \theta_d(t)$$

In order to calculate the feed-forward part, $\mathbf{g_R}(t)$ in equation (18), $\theta_d(t+t_p)$ from present time to 0.3 seconds ahead of the desired state vector, $\mathbf{x_d}(t)$ are required in each time frame. Since the dissertation (Youn, 1992) shows that 0.3 seconds preview time is suitable to get full advantage of preview information, predicting time is selected as 0.3 seconds. The $\mathbf{g_R}(t)$ is computed corresponding to each of three methods to get $\theta_d(t+t_p)$. The computer simulation performance results for each $\mathbf{g_R}(t)$ are analyzed and compared to one another. Two different simulation conditions were applied in order to evaluate the roll motion performances of the system according to desired $\theta_d(t+t_p)$ predicted by each of the three different methods.

The first condition, as illustrated in Figure 6 (a), simulates the vehicle traveling at 80km/hour on an S-shaped road with 300 m radius of curvature. Figure 6 (b) shows that the passive system is directly affected by the centrifugal body force, which causes the vehicle to tilt radially outward. The active system with each of the three methods would attempt to tilt towards the opposite direction in efforts to cancel out the centrifugal force acting upon the passengers. Although all three methods follow the desired angle closely, the system using method 1 reacts earlier and better than the systems using the other two methods.

The second condition, as illustrated in Figure 7 (a), is similar to the first but with the 3° banked road. For simplicity and clarity, road is flat when straight, but the 3° banked road is applied as soon as the curve begins. As Figure 7 (b) shows, the passive system is affected by both the centrifugal body force and the 3° banked road, resulting in the steady state of the vehicle angle to be approximately 2°. Since the angle of the car body is measured with respect

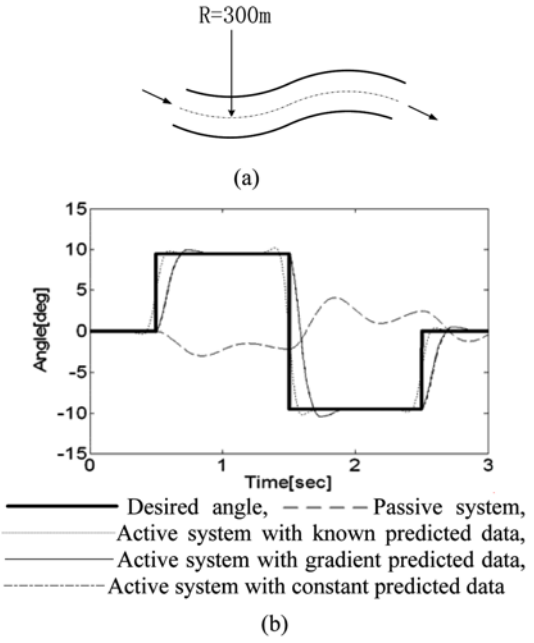

Figure 6. Roll angles of a car body traveling at 80 km/hour speed on the S-shaped flat faced road with a radius of 300 m: (a) S-shaped flat faced road; (b) Roll angles of a car body.

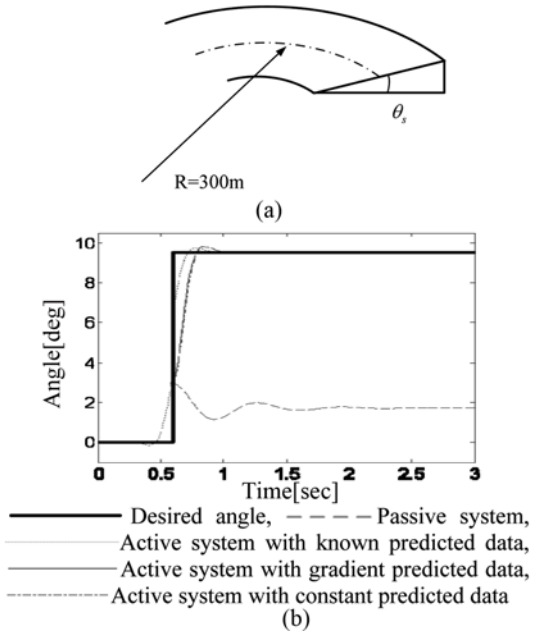

Figure 7. Roll angles of a car body traveling at 80 km/hour on the circular path with 3 degree banked road: (a) Circular banked road; (b) Roll angles of a car body.

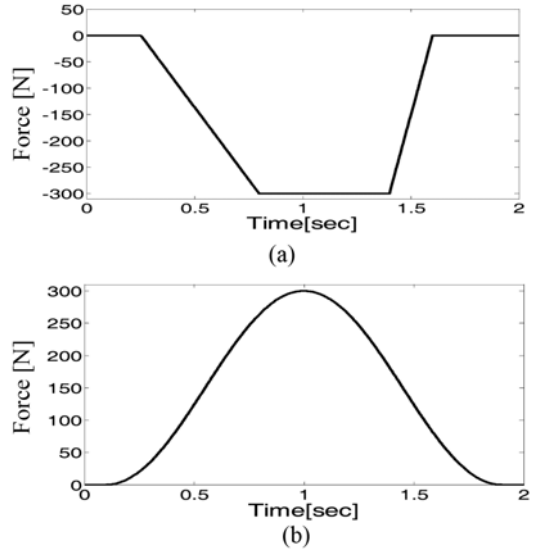

Figure 8. Braking and accelerating forces applied to a car body on the flat faced road: (a) Braking force; (b) Accelerating force.

to the horizontal level, the desired angle of the car body remains the same as in Figure 6 (b). In other words, the active suspension system tilts the vehicle body by desired angle subtracted by 3° banked road angle. Method 1 still shows the best results compared to the other two methods.

When a vehicle is braking or accelerating, the amount of inertial forces acting upon the vehicle can deteriorate the ride-comfort and handling capability. A solution to this problem is to counter the inertial forces by allowing the vehicle to pitch forward or backward.

Figure 8 shows suitably chosen amounts of braking and accelerating forces applied to the vehicle in each pitch motion simulation. The results of the simulations on the flat surface are shown in Figure 9.

The expected result is that the vehicle pitches backward when braking and forward when accelerating. This simulation also compares the differences in results from using each of three methods to calculate $\theta_d(t+t_p)$ where each method has its own pros and cons. The method 1 can create the best match to the desired angle. The method 2 can closely match the ideal angle with almost no delay, but it creates a slight overshoot due to the use of gradient. The method 3 does not create such overshoot, but it shows a relatively large delay compared to the other two methods. Though method 1 provides the best match to the desired angle, it is difficult to assume that the amount of braking and accelerating forces are predetermined in actual system. It would be a future challenge to find an algorithm to make the best estimation for $\theta_d(t+t_p)$.

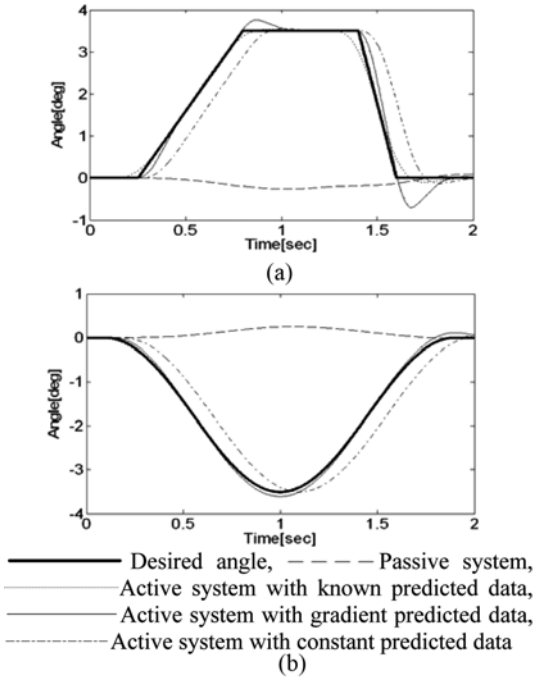

Figure 9. Pitch angles of a car body traveling with braking force and accelerating force on flat faced road: (a) Responses to braking force; (b) Responses to accelerating force.

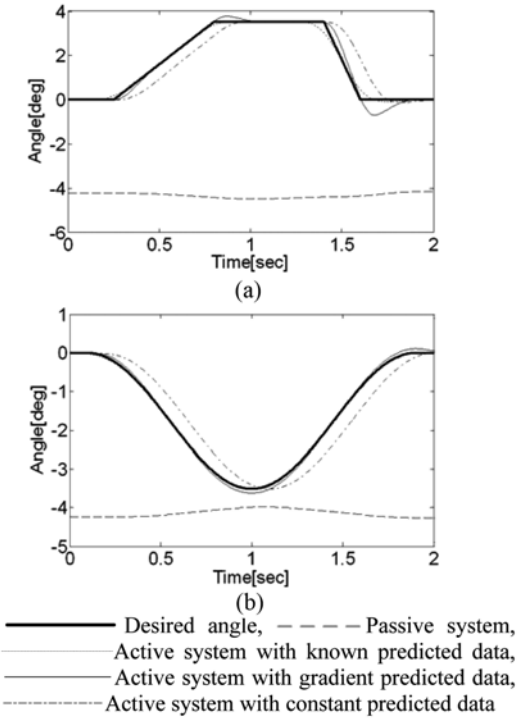

Figure 10. Pitch angles of a car body traveling with braking force and accelerating force on -4 degree ramp road: (a) Responses to braking force; (b) Responses to accelerating force.

The angle of the ground level on which the vehicle is placed is also an important factor to be considered. When the vehicle is traveling at a constant velocity on a steep downhill, a passive system cannot prevent the passengers from feeling uncomfortable. In contrast, an active system is able to negate this effect by setting the pitch angle of the vehicle body to be parallel to the horizontal plane. As shown in Figure 10, the ideal pitch angle of the vehicle body traveling –4° downslope is 0°. When the vehicle is moving uphill, however, it is not necessary to make additional adjustments to the pitch angle of the vehicle body because the passenger is comfortably leaning on the back of the seat. Thus the ideal pitch angle of the vehicle body is set parallel to the surface of the road.

Figure 11 illustrates the effects of acceleration and deceleration on the vehicle body traveling up the 10° ramped road with each type of systems. For both positive and negative slope simulations, the overall performance results of $\theta_d(t+t_p)$ obtained by each of the three methods are similar to the results from Figure 9. The exact calculation procedure of the ideal pitch angle is illustrated by equation (7). On a side note, it is apparent in Figure 11 that the passive system causes the pitch angle of the vehicle body to be slightly greater than the slope of the road. This is due to the vehicle's center of mass being shifted toward the rear.

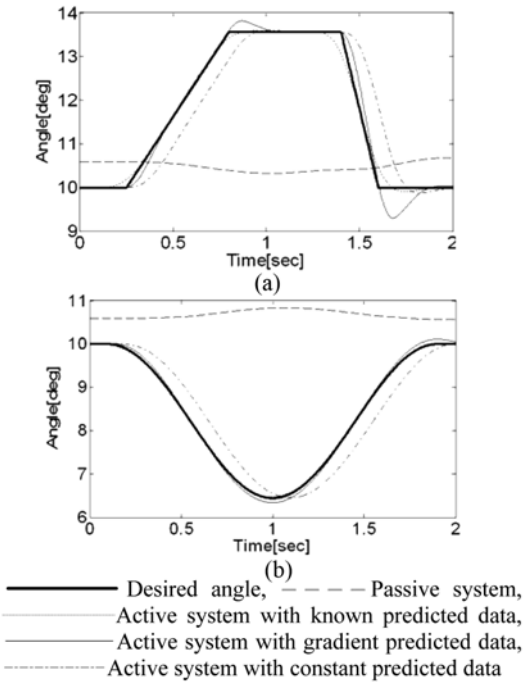

Figure 11. Pitch angles of a car body traveling with braking force and accelerating force on 10 degree ramp road: (a) Responses to braking force; (b) Responses to accelerating force.

6. CONCLUSION

In this study, the optimal tracking controllers with active suspension systems are designed for the purpose of following the ideal attitude motion of a car body. The simulation results under various different situations show that the optimal tracking controller makes the actual motion of a car body follow the desired motion with a little difference depending on the three kinds of predicted data. Therefore, the proposed tracking attitude controller consisting of feedback and feed-forward parts can obviously improve the ride-comfort and the handling capability simultaneously by controlling attitude motion of a car body at cornering, braking, and accelerating.

ACKNOWLEDGEMENT–This research was supported by Grant No. 2009-0073906 of National Research Foundation of Korea.

REFERENCES

Cho, B. K., Ryu, G. and Song, S. J. (2005). Control strategy of an active suspension for a half car model with preview information. *Int. J. Automotive Technology* **6**, **3**, 243–249.

Gaspar, P., Szaszi, I. and Bokor, J. (2005). Reconfigurable control structure to prevent the rollover of heavy vehicles. *Control Engineering Practice*, **13**, 699–711.

Goodall, R. M. (1999). Tilting trains and beyond-The future for active railway suspensions: Part 1. *Improving Passenger Comfort, J. Comput. Control Eng.* **10**, **4**, 153–160.

Malekshahi, A. and Mirzaei, M. (2012). Designing a non-linear tracking controller for vehicle active suspension systems using an optimization process. *Int. J. Automotive Technology* **13**, **2**, 263–271.

Shen, G. J., Liu, Z. Q. and Meng, L. J. (2000). Analysis of the longitudinal dynamics test on No. T41/42 train from West Beijing Station to Xi'an Station. *Roll. Stock* **40**, **11**, 8–9.

Wang, J. and Shen, S. W. (2008). Integrated vehicle ride and roll control via active suspensions. *Vehicle System Dynamics*, **46**, 495–508.

Wu, Z. H., Liu, Y. F. and Pan, G. (2009). A smart car control model for brake comfort based on car following. *IEEE Trans. Intelligent Transportation Systems* **10**, **1**, 42–46.

Youn, I. (1992). *Optimal Control of Semi-Active Automobile Suspension Including Preview Information.* Ph. D. Dissertation. State University of New York at S.B.

Youn, I., Im, J. and Tomizuka, M. (2006). Level and attitude control of the active suspension system with integral and derivative action. *Vehicle System Dynamic*, **44**, 659–674.

Youn, I. and Hac, A. (2006). Preview control of active suspension with integral action. *Int. J. Automotive Technology* **7**, **5**, 547–554.

APPENDIX

Nonzero elements of $A_{(10x10)}$ matrix are given as follows:

$$a_{1,1}=1$$
$$a_{2,1}=-(k_{s1}+k_{s2})/M,\ a_{2,2}=-(b_{s1}+b_{s2})/M$$
$$a_{2,3}=-(k_{s1}a-k_{s2}b)/M,\ a_{2,4}=-(b_{s1}a-b_{s2}b)/M$$
$$a_{2,6}=b_{s1}/M,\ a_{2,8}=b_{s2}/M$$
$$a_{2,9}=k_{s1}/M,\ a_{2,10}=k_{s2}/M$$
$$a_{3,4}=1$$
$$a_{4,1}=-(k_{s1}a-k_{s2}b)/I,\ a_{4,2}=-(b_{s1}a-b_{s2}b)/I$$
$$a_{4,3}=-(k_{s1}a^2+k_{s2}b^2)/I,\ a_{4,4}=-(b_{s1}a^2+b_{s2}b^2)/I$$
$$a_{4,6}=b_{s1}a/I,\ a_{4,8}=-b_{s2}b/I$$
$$a_{4,9}=k_{s1}a/I,\ a_{4,10}=-k_{s2}b/I$$
$$a_{5,7}=1$$
$$a_{6,1}=k_{s1}/m_1,\ a_{6,2}=b_{s1}/m_1,\ a_{6,3}=k_{s1}a/m_1$$
$$a_{6,4}=b_{s1}a/m_1,\ a_{6,5}=-k_{t1}/m_1$$
$$a_{6,6}=-b_{s1}/m_1,\ a_{6,9}=-k_{s1}/m_1$$
$$a_{7,8}=1$$
$$a_{8,1}=k_{s2}/m_2,\ a_{8,2}=b_{s2}/m_2,\ a_{8,3}=-k_{s2}b/m_2$$
$$a_{8,4}=-b_{s2}b/m_2,\ a_{8,7}=-k_{t2}/m_2$$
$$a_{8,8}=-b_{s2}/m_2,\ a_{8,10}=-k_{s2}/m_2$$
$$a_{9,6}=1,\ a_{10,8}=1$$

Elements of $\mathbf{B}_{(10x2)}$ and $\mathbf{D}_{(10x4)}$ matrix are given as follows

$$\mathbf{B}=\begin{bmatrix} 0 & 0 \\ 1/M & 1/M \\ 0 & 0 \\ a/I & -b/I \\ 0 & 0 \\ -1/m_1 & 0 \\ 0 & 0 \\ 0 & -1/m_2 \\ 0 & 0 \\ 0 & 0 \end{bmatrix} \quad \mathbf{D}=\begin{bmatrix} 0 & 0 & 0 & 0 \\ 0 & 0 & 1/M & 1/M \\ 0 & 0 & 0 & 0 \\ 0 & 0 & a/I & -b/I \\ -1 & 0 & 0 & 0 \\ 0 & 0 & 0 & 0 \\ 0 & -1 & 0 & 0 \\ 0 & 0 & 0 & 0 \\ 0 & 0 & 0 & 0 \\ 0 & 0 & 0 & 0 \end{bmatrix}$$

Elements of $\mathbf{Q}_{(10x10)}$ matrix are given as follows.

$$q_{i,j} = \rho_1 a_{2,i} a_{2,j} + \rho_2 a_{4,i} a_{4,j}$$

Specially,

$$q_{1,1} = \rho_1 a_{2,1} a_{2,1} + \rho_2 a_{4,1} a_{4,1} + 2\rho_3$$
$$q_{1,3} = \rho_1 a_{2,1} a_{2,3} + \rho_2 a_{4,1} a_{4,3} + \rho_3 (a-b)$$
$$q_{1,9} = \rho_1 a_{2,1} a_{2,9} + \rho_2 a_{4,1} a_{4,9} - \rho_3$$
$$q_{1,10} = \rho_1 a_{2,1} a_{2,10} + \rho_2 a_{4,1} a_{4,10} - \rho_3$$

$$q_{3,3} = \rho_1 a_{2,3} a_{2,3} + \rho_2 a_{4,3} a_{4,3} + \rho_3 (a^2 + b^2) + \rho_4$$
$$q_{3,9} = \rho_1 a_{2,3} a_{2,9} + \rho_2 a_{4,3} a_{4,9} - \rho_3 a$$
$$q_{3,10} = \rho_1 a_{2,3} a_{2,10} + \rho_2 a_{4,3} a_{4,10} + \rho_3 b$$
$$q_{5,5} = \rho_1 a_{2,5} a_{2,5} + \rho_2 a_{4,5} a_{4,5} + \rho_5$$

$$q_{7,7} = \rho_1 a_{2,7} a_{2,7} + \rho_2 a_{4,7} a_{4,7} + \rho_5$$
$$q_{9,9} = \rho_1 a_{2,9} a_{2,9} + \rho_2 a_{4,9} a_{4,9} + \rho_3$$
$$q_{10,10} = \rho_1 a_{2,10} a_{2,10} + \rho_2 a_{4,10} a_{4,10} + \rho_3$$

where, a is an element of **A** matrix, i=1~10, j=1~10

$\mathbf{N1}_{(10x2)}$ matrix is defined as follows.

$$n_{1_{i,j}} = \rho_1 a_{2,i} b_{2,j} + \rho_2 a_{4,i} b_{4,j}$$

where, a and b are elements of **A** and **B** matrixes, i=1~10, j=1~2.

$\mathbf{N2}_{(10x4)}$ matrix is defined as follows.

$$n_{2_{i,j}} = \rho_1 a_{2,i} a_{2,j} + \rho_2 a_{4,i} d_{4,j}$$

where, a and $d$are elements of **A** and **D** matrixes, i=1~10, j=1~4

$\mathbf{R}_{(2x2)}$ matrix is defined as follows.

$$\begin{bmatrix} r_{1,1}+\rho_6 & r_{1,2} \\ r_{1,2} & r_{2,2}+\rho_6 \end{bmatrix}$$

where, $r_{i,j} = \rho_1 b_{2,i} b_{2,j} + \rho_2 b_{4,i} b_{4,j}$, b is an element of **B**

$\mathbf{M1}_{(4x2)}$ matrix is defined as follows.

$$m_{1_{i,j}} = \rho_1 d_{2,i} b_{2,j} + \rho_2 d_{4,i} b_{4,j}$$

where, b and d areelements of **B** and **D** matrixes, i=1~4, j=1~2

$\mathbf{M2}_{(4x4)}$ matrix is defined as follows.

$$m_{2_{i,j}} = \rho_1 d_{2,i} d_{2,j} + \rho_2 d_{4,i} d_{4,j}$$

where, d is an element of **D** matrixes, i=1~4, j=1~4